https://doi.org/10.5194/egusphere-2026-3795
Preprint. Discussion started: 29 July 2026

Data-driven Tide Correction for SAR-derived Ice Velocity Measurements on Antarctic Ice Shelves

Yikai Zhu[1], Anna E. Hogg[1], Benjamin J. Wallis[1], Ross A.W. Slater[1], Oliver J. Marsh[2]

[1]School of Earth, Environment & Sustainability, University of Leeds, Leeds, LS2 9JT, United Kingdom
[2]British Antarctic Survey, Cambridge, CB3 0ET, United Kingdom

Correspondence to: Yikai Zhu (Y.Zhu3@leeds.ac.uk)

Abstract. Synthetic Aperture Radar (SAR) offset tracking is widely used to measure ice velocity on floating ice shelves, however, vertical displacement caused by ocean tides projects into the radar-range direction, introducing apparent horizontal motion unrelated to true ice flow. Here, we develop an observation-driven tide-correction for SAR-derived ice speed measurements using differential range offset tracking (DROT) applied to Sentinel-1 SAR data. The method estimates spatially and temporally varying tidal response coefficients directly from observed radar-range displacement variability and an ocean tide model. Application of the method to SAR-derived ice velocity measurements on Antarctic Ice Shelves shows spatial variability in the magnitude of the tide-induced ice-speed correction, with an Antarctic-wide mean tide-correction range of 106 m/yr, a standard deviation of 71 m/yr and maximum values exceeding 300 m/yr. The largest tide correction range predominantly occurs on freely floating ice shelves in regions of strong tidal forcing, particularly in the Weddell Sea and Antarctic Peninsula. Smaller tide corrections are observed near grounding zones and pinned regions where tidal motion is mechanically constrained. Time-series analyses show that the tide correction systematically reduces non-physical temporal variability in SAR-derived ice velocity products while preserving the large-scale spatial structure of ice flow. Independent validation using GNSS observations on Brunt Ice Shelf shows improved agreement between tide-corrected satellite-based ice speed and in situ measurements. Our results demonstrate that tide-induced apparent motion is a source of variability in SAR-derived ice velocity products on floating ice shelves, highlighting the importance of applying a correction when tide-induced signals are not required.

1 Introduction

Ice motion is one of the most direct, low-latency, and informative expressions of glacier and ice-sheet dynamics (Rignot et al., 2011; Dirscherl et al., 2020). Variations in ice velocity reflect changes in driving stress, basal resistance, ice-ocean interaction, and internal deformation, and therefore provide essential constraints on ice discharge and mass balance (Hogg et al., 2017; Shepherd et al., 2018; Rignot et al., 2019; Shepherd et al., 2020; Davison et al., 2023; Otosaka et al., 2023). Reliable measurements of ice flow are fundamental for assessing the contribution of land ice to sea-level rise and for identifying dynamical instabilities that may precede rapid change (van de Wal et al., 2008; McMillan et al., 2014; Lemos et al., 2018;

https://doi.org/10.5194/egusphere-2026-3795
Preprint. Discussion started: 29 July 2026

Wallis et al., 2023b). Beyond mass balance estimation, spatial gradients in velocity underpin strain-rate analyses and are widely used in ice-flow modelling, inference of basal conditions, grounding-zone investigations and monitoring of calving and rift propagation (Joughin et al., 2009; Bassis and Jacobs, 2013; Alley et al., 2018; Benn et al., 2022). Sustained, spatially extensive velocity observations are thus critical for detecting such short-term variability and long-term trends in ice dynamics. Satellite synthetic aperture radar (SAR) has transformed ice velocity mapping by enabling systematic, all-weather observations across Antarctica and Greenland (Rignot et al., 2011; Nagler et al., 2015; Joughin et al., 2018; Solgaard et al., 2021; Wuite et al., 2026). In particular, the European Space Agency (ESA) and European Commission (EC) Copernicus Sentinel-1 mission has fundamentally advanced continent-scale ice velocity monitoring through its near-continuous acquisition strategy, wide spatial coverage and short revisit interval. Differential interferometry (Rignot, 1996; Palmer et al., 2009; Gourmelen et al., 2011) and offset tracking (Strozzi et al., 2003; Lemos et al., 2018; Wallis et al., 2023b; Selley et al., 2025; Wuite et al., 2026) now provide routinely updated measurements of Antarctic ice motion with unprecedented temporal consistency. Offset tracking is especially important over floating ice shelves, where decorrelation due to surface melt and fast ice flow often limits interferometric approaches, but broad spatial coverage remains essential.

The increasing availability of short-repeat (weekly) Sentinel-1 observations has greatly improved the capability to investigate short-term ice-dynamic variability in Antarctica (Boxall et al., 2022; Wallis et al., 2023b), but it has also highlighted the sensitivity of SAR-derived offset tracking measurements to non-horizontal motion (Rott et al., 2020). Over floating ice in particular, measured surface displacements reflect not only horizontal ice motion but also vertical displacement induced by ocean tides and variations in atmospheric air pressure (Padman et al., 2003; Vaughan, 1995). When successive SAR acquisitions occur at different tidal stages, vertical motion is projected into the radar range direction and produces an apparent horizontal offset unrelated to true ice flow. This may lead to a bias in the ice velocity measurement, which although less apparent in long-term (annual) ice speed mosaics when the full tide cycle is represented, is significant when considering short-term (weekly) ice speed variability (Marsh et al., 2013). Without an appropriate correction, tide-induced apparent motion can obscure sub-annual ice-dynamic variability and complicate interpretation of velocity changes near grounding lines and pinning points.

The tidal response of floating ice shelves is spatially heterogeneous and governed by several physical controls. Near grounding zones, vertical motion is constrained by basal contact and the rigidity of ice, which produces a flexural gradient that attenuates tidal displacement relative to freely floating ice (Vaughan, 1995; Padman et al., 2003). Seaward of the grounding line, tidal sensitivity increases as basal constraint diminishes and the ice shelf approaches hydrostatic equilibrium (Fricker and Padman, 2006; Brunt et al., 2011). Ice thickness further modulates this behaviour through its control on flexural rigidity. Thicker ice shelves resist bending and exhibit smoother spatial gradient in vertical deflection, whereas thinner ice responds more directly to tidal forcing leading to a narrower hinge zone between grounded ice and hydrostatic equilibrium (Marsh et al., 2014; Dawson and Bamber, 2020). Additional complexity arises from local bathymetry, lateral confinement, and the presence of pinning

https://doi.org/10.5194/egusphere-2026-3795
Preprint. Discussion started: 29 July 2026

points, which may locally suppress or redistribute tidal flexure (Fürst et al., 2016; Reese et al., 2018; Miles and Bingham, 2024). As a result, the relationship between tidal height variability and radar-range displacement varies substantially across Antarctic ice shelves and therefore represents a major challenge for continent-scale tide correction of SAR-derived ice velocity products.

Existing tide correction strategies differ in implementation but share a common objective: determining how strongly a given location on a floating ice shelf responds to tidal forcing and how this response translates into radar-range displacement. Physically parameterized schemes, such as those implemented in ESA Climate Change Initiative (CCI) ice velocity products (Wuite et al., 2026), estimate tidal sensitivity from elastic beam theory by relating vertical deflection to ice thickness and distance from the grounding line (Vaughan, 1995). This approach provides a physically interpretable framework and enables large-scale application. However, its performance depends on the accuracy of external inputs such as ice thickness and grounding line position, as well as assumptions regarding material properties including Young's modulus. Both the geometry and mechanical properties of ice shelves may evolve through time due to grounding line migration, ice shelf thinning and calving-related changes in ice shelf structure. Because tidal flexure depends strongly on these parameters, uncertainties in the prescribed geometry may influence the estimated tidal response. Interferometric approaches estimate tidal sensitivity empirically from phase measurements by regressing observed line-of-sight displacement against modelled tidal height differences (Han and Lee, 2015). While this method directly captures grounding zone flexure from observations, its applicability is often constrained by coherence conditions and the availability of suitable interferometric pairs. Despite the widespread use of offset tracking for Antarctic ice velocity measurements, observation-driven approaches specifically designed to estimate and correct tide-induced apparent motion in offset-derived ice velocity products remain limited.

In this study, we develop a data-driven framework for tide correction of offset-tracking ice velocities based on differential range offset tracking (DROT) (Marsh et al., 2013; Hogg, 2015; Zhu et al., 2025). By analysing differential range-direction offsets derived from Sentinel-1 time series, the approach reduces the influence of horizontal ice motion and isolates the component of displacement associated with vertical motion. This enables a direct estimation of the relationship between tide-driven sea-surface height variability and radar-measured offsets. In contrast to physically parameterized approaches, this framework does not rely on external geometric inputs such as ice thickness or grounding line position but instead derives tidal response directly from repeated observations. We evaluate the framework using Antarctic-wide Sentinel-1 observations together with representative ice shelves spanning contrasting tidal regimes, including Pine Island, Larsen C, Brunt Stancomb, and Shackleton Ice Shelves. Tide-corrected ice speed measurements are further compared with independent Global Navigation Satellite System (GNSS) observations over Brunt Stancomb Ice Shelf to assess the reduction of tide-induced apparent motion. Through these analyses, we investigate how alternative representations of tidal response influence SAR-derived ice speed measurements across Antarctic Ice Shelves.

https://doi.org/10.5194/egusphere-2026-3795
Preprint. Discussion started: 29 July 2026

2 Methods and Data

2.1 Ice Speed Measurements from Sentinel-1

Ice velocity is derived from Sentinel-1 SAR imagery using offset tracking techniques (Strozzi et al., 2003; Marsh et al., 2013; Hogg, 2015; Joughin et al., 2016; Wuite et al., 2026). We use Level-1 Single Look Complex (SLC) data acquired in Interferometric Wide (IW) swath mode which uses a Terrain Observation by Progressive Scans (TOPS) operational mode (De Zan and Guarnieri, 2006). For our observations, we use the full archive of these data from October 2014 to December 2025, which includes near total coverage of the AIS margin from 2017 onwards. We use all 6 and 12-day separated acquisition pairs, noting that this repeat period is variable between different satellite ground tracks through time. Most notably, 6-day repeats are only available during periods of two or more active Sentinel-1 satellite platforms, between September 2016 to December 2021 and March 2025 onwards.

Surface displacement between acquisitions is estimated through intensity-based feature tracking by maximising the cross-correlation of image patches in the range and azimuth directions (Strozzi et al., 2003). This approach exploits persistent backscatter patterns such as crevasses, rifts and speckle structures, and is therefore well suited to floating ice shelves where interferometric coherence is often limited. Compared with interferometric methods, offset tracking is less sensitive to temporal decorrelation, can produce a 2-D velocity field from a single satellite ground track and enables robust ice velocity retrieval over large spatial scales. Prior to velocity tracking, repeat-pass SAR images are co-registered using precise orbit information and the Reference Elevation Model of Antarctica (REMA) v2 digital elevation model (DEM) (Howat et al., 2019, 2022), after which range and azimuth offsets are estimated for sequential image pairs. These offsets are converted to ground-range displacements using the imaging geometry and the DEM and ice velocity is obtained by dividing displacement by the temporal separation between acquisitions. Quality control is applied to exclude low-correlation matches and non-ice areas, resulting in spatially continuous velocity fields across Antarctic Ice Shelves. This processing chain is consistent with previous studies (Hogg et al., 2017; Lemos et al., 2018; Selley et al., 2021; Davison et al., 2023; Wallis et al., 2023b; Davison et al., 2025).

2.2 Geometric Origin of Tidal Signal

Offset tracking measures displacement in radar geometry, therefore the retrieved ice speed field includes contributions from motion projected into the radar line of sight. Over floating ice shelves, vertical displacements induced by ocean tides are projected into the radar range direction and can therefore introduce an apparent horizontal displacement unrelated to true flow (Figure 1a). When two SAR acquisitions occur at different tidal states, the resulting vertical tidal difference between the acquisition times produces an apparent horizontal displacement in the radar range direction (Marsh et al., 2013; Friedl et al., 2020). For a radar incidence angle θ, the tidal-induced ground-range displacement S associated with a tidal difference $\zeta_1 - \zeta_2$ can be approximated as

https://doi.org/10.5194/egusphere-2026-3795
Preprint. Discussion started: 29 July 2026

$$S = \frac{\zeta_1 - \zeta_2}{tan\theta} \quad (1)$$

This geometric projection causes vertical tidal motion of the ice shelf surface to appear as horizontal displacement in offset-tracking measurements. Consequently, the displacement measured between two SAR images contains both the true horizontal ice motion and an additional component related to tidal elevation differences.

The typical peak-to-peak tidal range on most Antarctic Ice Shelves is approximately 1-2 m, increasing to 2-4 m during spring tides and occasionally exceeding 6 m in some regions (Padman et al., 2002). For repeat intervals typical of Sentinel-1 acquisitions, such tidal amplitudes can generate radar-range displacements of decimetre scale (Wallis et al., 2024; Zhu et al., 2025), leading to velocity biases that are significant when considering short-term ice speed variability.

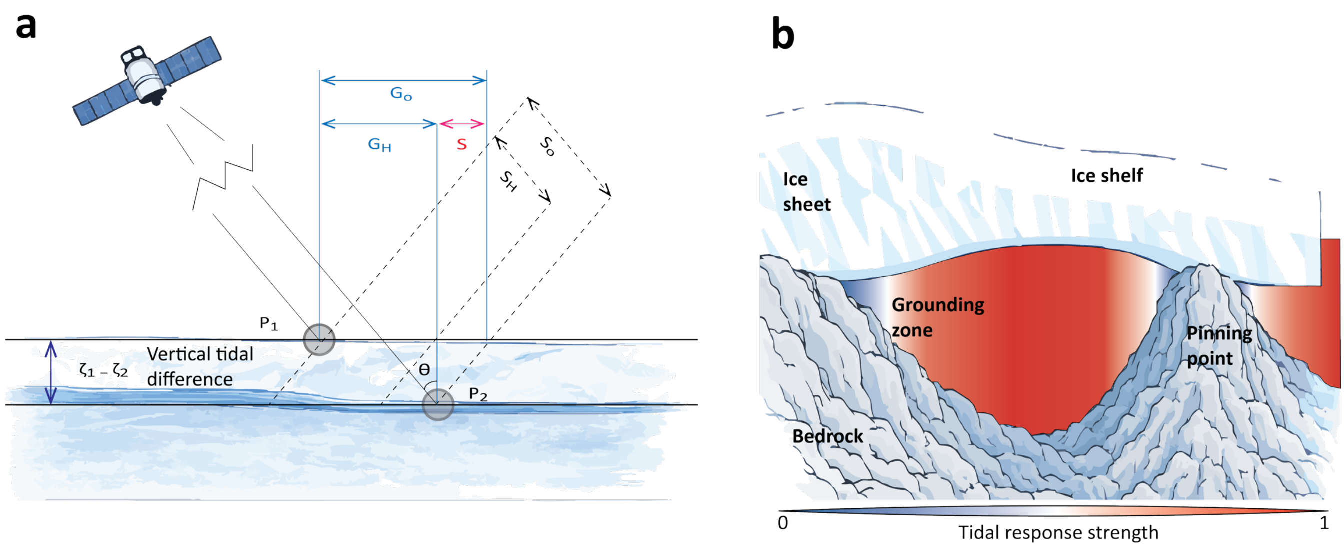

Figure 1. Illustration of tide signal in SAR-derived ice velocity measurements and spatial variability of tidal response over floating ice shelves. (a) Imaging geometry of a side-looking satellite SAR system illustrating how vertical tidal motion impacts floating ice, introducing an apparent horizontal displacement in the radar range direction. When two SAR acquisitions occur at different tidal states, the resulting vertical tidal difference projects into the radar range direction and influences the measured ground-range displacement. The observed displacement (G_O) therefore consists of the true horizontal ice motion (G_H) and an additional tidal projection component (S) related to the radar incidence angle. (b) Cross-sectional view of an Antarctic Ice Shelf system illustrating the spatial variability in tidal response. Near the grounding zone, the ice shelf remains partially supported by the bed and exhibits limited tidal motion (blue shading), while further downstream the floating ice shelf responds more freely to ocean tides (red shading). Local pinning points provide additional basal resistance and reduce local tidal flexure, producing spatial heterogeneity in tidal response across the ice shelf.

2.3 DROT-based Tide Correction

The tidal response of Antarctic Ice Shelves is spatially heterogeneous and varies according to local grounding conditions, flexural behaviour, and basal resistance (Figure 1b) (Vaughan, 1995; Padman et al., 2003; Fürst et al., 2016; Padman et al., 2018; Reese et al., 2018). Near grounding zones, vertical tidal motion is suppressed because the ice shelf remains mechanically

https://doi.org/10.5194/egusphere-2026-3795
Preprint. Discussion started: 29 July 2026

coupled to grounded ice and experiences strong flexural resistance (Vaughan, 1995). In contrast, freely floating ice shelves generally exhibit larger tidal displacement amplitudes. Local pinning points may further reduce vertical motion by providing localized basal resistance and modifying surrounding flexural behaviour. Ice thickness, lateral confinement, and local bathymetry additionally influence how tidal forcing propagates across an ice shelf. Consequently, the relationship between sea-surface height variability and radar-range displacement varies substantially across Antarctic Ice Shelves and cannot be represented using a spatially or temporally uniform correction parameter.

To quantify this spatially varying tidal sensitivity, we define a tidal response coefficient ω, which describes how strongly local sea-surface height variability is expressed as displacement in radar geometry. The relationship between observed range displacement and sea-surface height change can be expressed as:

$$d_{\mathrm{range}} = \omega \cdot \Delta SSH + \epsilon \tag{2}$$

where d_{range} is the displacement measured in the radar range direction, ΔSSH is the sea-surface height difference between SAR acquisitions, and ϵ represents residual contributions from noise and unmodelled processes. The coefficient ω therefore represents the local tidal sensitivity of the ice shelf. Regions with limited tidal motion, such as grounding zones or strongly pinned areas, typically exhibit smaller values of ω, whereas freely floating ice shelves generally exhibit larger values. Ice floating in pure hydrostatic equilibrium with no mechanical coupling to the grounded ice sheet would be expected to have $\omega = 1$.

In this study, ΔSSH is derived from the CATS2008 tidal model (Padman et al., 2008; Howard et al., 2019), while atmospheric pressure effects are accounted for using inverse barometer correction estimated from ERA5 pressure dataset (Hersbach et al., 2023). This resulting sea-surface height variability therefore includes contributions from both ocean tides and atmospheric forcing and is calculated for each Sentinel-1 SAR image acquisition time.

The tidal response coefficient is estimated empirically using differential range offset tracking (DROT) applied to the Sentinel-1 time series (Joughin et al., 2016; Wallis et al., 2024; Zhu et al., 2025). Offset tracking provides range offsets that contain contributions from both horizontal ice motion and vertical tide-induced displacement. Because horizontal ice flow generally varies smoothly over short spatial scales, neighbouring pixels tend to exhibit similar background motion. In contrast, tidal flexure produces localized spatial gradients in vertical displacement, particularly near grounding zones and pinning points where tidal response changes rapidly over distance. By differencing temporally adjacent range offsets, DROT suppresses the long-wavelength component of steady horizontal motion while preserving localized gradients associated with tidal flexure. This enables direct isolation of tide-related displacement signals in radar geometry and helps resolve spatial patterns associated with tidal response variability.

https://doi.org/10.5194/egusphere-2026-3795
Preprint. Discussion started: 29 July 2026

For each pixel, ω is estimated by regressing differential range offsets against temporal differences in pair-wise sea-surface height differences, denoted as ($\Delta(\Delta SSH)$), across the Sentinel-1 time series. The resulting coefficient field therefore reflects the observed local flexural behaviour of the ice shelf without requiring external information on ice thickness, grounding-line position, or pinning-point geometry. The derived tidal response coefficient forms the basis for the tide-correction procedure described in the following section.

2.4 Implementation of Tide Correction

The estimated tidal response coefficient is applied to individual Sentinel-1 image pairs to correct tide-induced displacement in the radar range direction (Figure 2). For each SAR pair, offset tracking is first applied to derive azimuth and range offsets in radar geometry, as described above. Differential range offsets are subsequently constructed from the range-offset time series and used together with modelled sea-surface height variability to estimate the tidal response coefficient through pixel-wise regression. In parallel, sea-surface height differences are calculated from the CATS2008 tidal model and ERA5-based inverse barometer corrections using the precise acquisition time of the input images. The estimated tidal response coefficient is then combined with sea-surface height differences and the local radar incidence map to calculate range-direction tide corrections for each SAR image pair. These corrections are applied directly to the original range offsets, producing tide-corrected range displacement fields while preserving the original azimuth offsets derived from offset tracking. Because the tidal contribution primarily projects into the radar range direction, azimuth offsets are assumed to be minimally affected by vertical tidal motion and are therefore retained unchanged during the correction procedure. The corrected range offsets are subsequently recombined with the azimuth offsets using the SAR image geometry and local incidence angle information to derive tide-corrected horizontal velocity components (Vx and Vy). Final ice-speed magnitude is then calculated from the corrected velocity components. The correction is applied independently to each Sentinel-1 image pair and supports both 6-day and 12-day repeat intervals.

Once the tidal response coefficient has been estimated from the historical Sentinel-1 archive, application of the correction to newly acquired Sentinel-1 image pairs requires only the updated sea-surface height differences derived from the tidal model and inverse barometer correction. Consequently, extending the correction to future Sentinel-1 observations does not require reprocessing of the complete historical SAR archive. The most computationally demanding component of the workflow remains the original SAR offset tracking processing, whereas the tide correction itself involves only a pixel-wise application of the pre-computed tidal response coefficient and therefore introduces relatively little additional computational overhead.

https://doi.org/10.5194/egusphere-2026-3795
Preprint. Discussion started: 29 July 2026

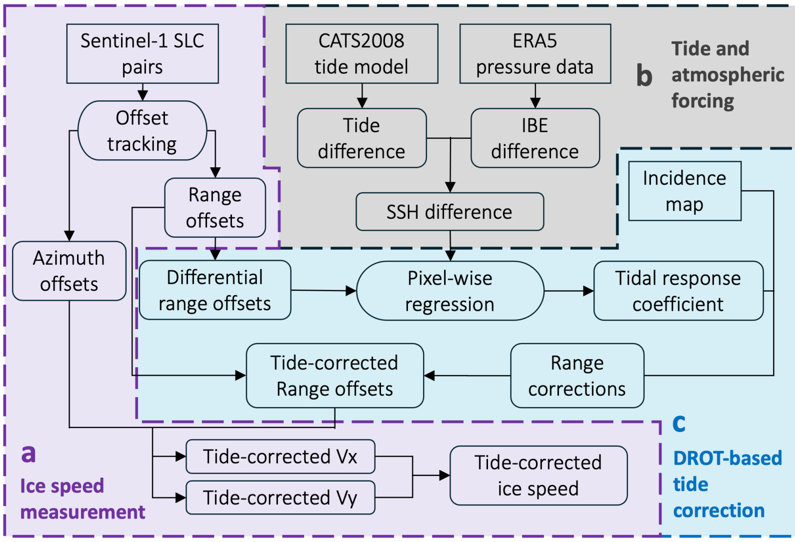

Figure 2. Workflow of the DROT-based tide correction framework for Antarctic ice speed measurements. The workflow consists of three major components: (a) ice speed measurement from Sentinel-1 SAR image pairs using offset tracking, (b) construction of external tidal and atmospheric forcing fields from the CATS2008 tide model and ERA5 air pressure data, and (c) DROT-based tide correction. Rectangular boxes denote input datasets, rounded boxes represent intermediate and final products, elongated rounded boxes indicate processing steps, and dashed outlines delineate the three major components of the workflow.

3 Results

3.1 Antarctic Tide Correction Range

The Antarctic-wide distribution of tide correction range, defined as the difference between the maximum and minimum pairwise tide corrections estimated from October 2014 to December 2025, exhibits substantial spatial variability across Antarctic Ice Shelves (Figure 3). Mean correction magnitude over all Antarctic Ice Shelves reaches 106 m/yr with a standard deviation of 71 m/yr, while the maximum observed correction exceeds 300 m/yr. Approximately 41 % of ice shelf pixels exhibit tide correction ranges larger than 100 m/yr, indicating that tide-induced ice speed biases are widespread across Antarctic Ice Shelves and may substantially influence short-timescale ice speed variability derived from SAR offset tracking.

https://doi.org/10.5194/egusphere-2026-3795
Preprint. Discussion started: 29 July 2026

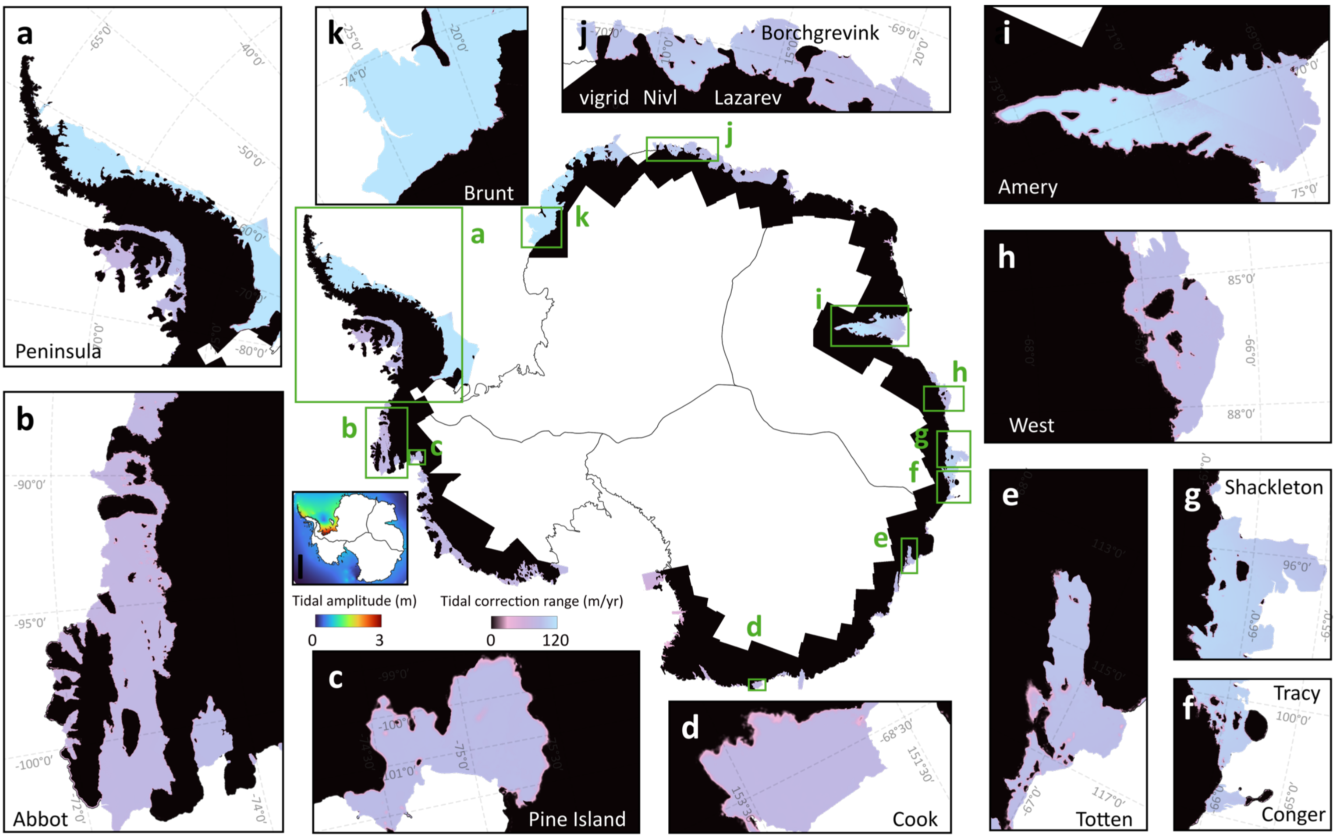

Figure 3. Spatial distribution of DROT-derived tide correction range on Antarctic Ice Shelves. The central panel shows the spatial distribution of tide correction range in Antarctica, defined as the difference between the maximum and minimum pairwise tide corrections estimated from Sentinel-1 SAR observations acquired between October 2014 and December 2025. The colour scale represents the magnitude of the tide correction range, with larger values indicating regions where tidal modulation exerts a stronger influence on observed ice shelf speeds. Green boxes indicate selected regions and ice shelves displayed in the surrounding zoomed-in panels, including: (a) Antarctic Peninsula; (b) Abbot; (c) Pine Island; (d) Cook; (e) Totten; (f) Tracy Tremenchus and Conger Glenzer; (g) Shackleton; (h) West; (i) Amery; (j) Nivl, Lazarev, and Borchgrevink; (k) Brunt Stancomb. Panel (l) shows the Antarctic tidal amplitude derived from the CATS2008 tidal model (Padman et al., 2008; Howard et al., 2019).

The largest tide correction ranges are primarily observed across large freely floating ice shelves in regions of strong tidal forcing, including several sectors of the Weddell Sea and Antarctic Peninsula where the tide correction can exceed 200 m/yr over extensive areas. In contrast, substantially smaller tide correction ranges are observed near grounding zones and locally pinned regions, where vertical tidal motion is mechanically constrained by basal contact and flexural resistance. Similar reductions are also evident around pinning points and confined embayment regions where the tidal response is locally suppressed, for example on the Southern margin of Totten Ice Shelf (Figure 3e). These spatial patterns broadly correspond to the Antarctic-wide distribution of DROT-derived tidal response coefficients (Figure S1), which generally increase from grounded regions toward fully floating ice shelves.

https://doi.org/10.5194/egusphere-2026-3795
Preprint. Discussion started: 29 July 2026

Regional differences in the magnitude of tide-induced velocity correction are pronounced. The Weddell Sea sector exhibits the largest overall tide corrections, with a mean magnitude of approximately 148 m/yr. In several regions of the Antarctic Peninsula the tide correction range locally exceeds 200 m/yr, producing some of the strongest spatial heterogeneity observed in Antarctica. For example, the neighbouring Larsen C and Larsen D Ice Shelves exhibit markedly different correction magnitudes despite their close geographic proximity (Figure 3a). By contrast, the Amundsen Sea Sector and Wilkes Land exhibit substantially smaller tide correction ranges, despite containing some of the most dynamically active glaciers in Antarctica. These regional differences primarily reflect spatial variations in tidal forcing, with regions that experience the largest tidal amplitude (Figure 3l) generally coinciding with the largest tide correction magnitude.

Importantly, large tide correction ranges are not restricted to narrow flexural transition zones but extend across extensive downstream portions of floating ice shelves. In regions where the total ice speed is slower flowing and the short-term ice speed variability is more modest, the estimated tide correction magnitude approaches the same order as observed short-term ice speed variability, suggesting that tide-induced offsets may obscure real short-term ice speed variability if a tide correction is not applied. As the apparent ice speed bias scales inversely with repeat interval, the effect is particularly important for short repeat SAR acquisitions, such as 6-day repeat Sentinel-1 or 1-day repeat Cosmo-SkyMed or ICEYE data, commonly used in Antarctic ice speed monitoring. These results demonstrate that tide-induced apparent motion constitutes a continent-wide source of variability in SAR-derived ice speed products that must be accounted for and highlights the importance of applying a temporally variable, spatially distributed tide correction to ice speed measurements on floating ice shelves.

3.2 Spatial Impact of Tide Correction Results

Representative examples from Pine Island, Larsen C, Brunt Stancomb, and Shackleton Ice Shelves illustrate the spatial impact of applying the tide correction to ice speed measurements on a range of Antarctic Ice Shelf settings (Figure 4). Together, these examples demonstrate that the magnitude of tide-induced ice speed signal is jointly controlled by three primary factors: the amplitude of tidal forcing, the local tidal response of the floating ice shelf, and the orientation of ice flow relative to the SAR viewing geometry. While the DROT-derived tidal response coefficient generally increases downstream of grounding zones as the ice becomes freely floating in hydrostatic equilibrium, the magnitude of the resulting correction varies substantially between Antarctic Ice Shelves because the tide amplitude differs strongly between regions and because the sensitivity of ice speed magnitude to range-direction corrections depends on the orientation of ice flow in the SAR image.

The contrast between Pine Island and Larsen C Ice Shelves clearly illustrates the differing influence of regional tidal forcing on SAR-derived ice speed measurements (Figure 4a and b). Both ice shelves exhibit elevated tidal response coefficients across downstream freely floating regions, indicating strong tidal coupling between ocean surface motion and radar-range displacement. At Pine Island Ice Shelf, differences between the raw and corrected ice speed remain close to zero across much of the main floating ice shelf (Figure 4a.iii), despite increasing tidal response downstream of the grounding line (Figure 4a.iv).

https://doi.org/10.5194/egusphere-2026-3795
Preprint. Discussion started: 29 July 2026

This is because tide amplitudes are relatively low in the Amundsen Sea Sector and the main trunk of Pine Island Glacier flows predominantly in the azimuth direction relative to the Sentinel-1 viewing geometry. Consequently, the range-direction tide correction signal is more dominant on the northern shelf region rather than the main fast flowing ice stream. For this reason, the profile shown in Figure 4a.iv was extracted across the northern shelf rather than along the glacier's main trunk. In contrast, a substantially larger tide correction is required on the Larsen C Ice Shelf as the tide amplitude in the Weddell Sea is nearly three times bigger than in the Amundsen Sea (Figure 4b.iii). Along-profile comparisons reveal progressively increasing separation between raw and tide-corrected ice speed profiles downstream of the grounding line, consistent with persistently elevated tidal response coefficients across the freely floating shelf (Figure 4b.iv). Together, the two examples demonstrate that elevated tidal response alone does not necessarily produce a large tide correction magnitude; instead, substantial tide-induced speed bias emerges where strong tidal response coincides with large tidal forcing.

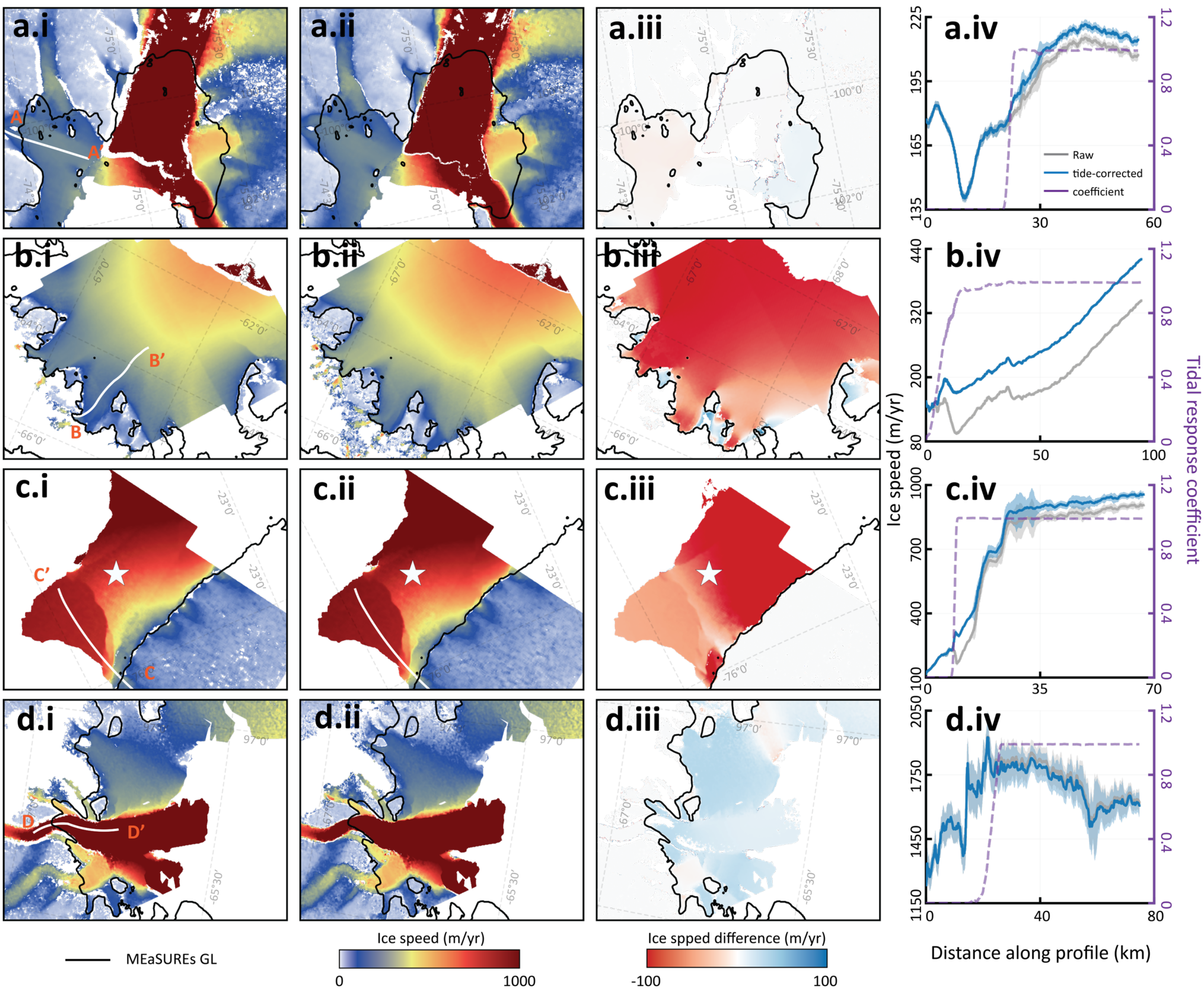

https://doi.org/10.5194/egusphere-2026-3795
Preprint. Discussion started: 29 July 2026

Figure 4. Spatial impact of applying the DROT-based tide correction to individual ice speed measurements in different regions of Antarctica. The panels show examples of the raw and tide-corrected ice speed measurements derived from individual Sentinel-1 SAR image pairs over four Antarctic Ice Shelves: (a) Pine Island; (b) Larsen C; (c) Brunt Stancomb; and (d) Shackleton. For each region, column (i) shows the original ice speed field before tide correction, column (ii) shows the DROT-based tide-corrected ice speed field, and column (iii) presents the ice speed difference between the raw and tide-corrected products. Column (iv) shows ice speed profiles extracted along the transects indicated in column (i), comparing raw (grey) and tide-corrected (blue) ice velocities. The dashed purple line represents the DROT-based tidal response coefficient along each profile. The white star in panel (c) indicates the location of the GNSS station used for independent validation. Black outlines indicate the MEaSUREs grounding line (Rignot et al., 2016). These examples are based on Sentinel-1 image pairs acquired on 24-30 May 2021 (Pine Island), 21-27 July 2021 (Larsen C), 8-14 September 2021 (Brunt Stancomb), and 3-9 November 2021 (Shackleton).

Brunt Stancomb Ice Shelf is an example of a region that requires a large ice speed tide correction due to its high ocean tide amplitude (Figure 4c). A large portion of the floating shelf requires a tide correction with a magnitude exceeding 100 m/yr (Figure 4c.iii), while the along-profile comparison further demonstrates the large tide correction values required over regions both near the grounding zone and downstream towards the freely floating calving front (Figure 4c.iv). The consistently elevated tidal response coefficient along the profile indicates that much of the ice shelf is floating in hydrostatic equilibrium and therefore responds freely to tidal forcing, allowing vertical tidal motion to project strongly into the radar-range direction. Under these conditions, tide-induced apparent motion introduces a broad and spatially coherent signal into the offset-tracking ice speed field. After the DROT-based tide correction is applied, the resulting ice speed measurement becomes visibly smoother and more internally consistent, indicating that a substantial fraction of the observed pair-scale variability originates from tidally induced differences between SAR image acquisitions, rather than true ice dynamic change. The Brunt Ice Shelf example also illustrates the importance of ice flow orientation relative to the SAR viewing geometry. As the tide-induced signal primarily affects the range-direction component of displacement, its influence on ice speed magnitude is strongest where ice motion contains a substantial range-direction component. Under such conditions, range-direction corrections translate directly into large changes in the total ice speed magnitude, contributing to the pronounced tide correction calculated for Brunt Stancomb Ice Shelf.

On Shackleton Ice Shelf, this region shows that measurable tide-induced ice speed signals are not only restricted to the largest Antarctic tidal regimes (Figure 4d). Although the ocean tide range in this region (approximately 1.5-1.8 m) is approximately half that on the Larsen C (3-4 m) or Brunt Stancomb (2.5-3 m) Ice Shelves, both the spatial difference map and the along-profile show a spatially coherent tide correction pattern on the floating shelf (Figure 4d.iii-iv). This indicates that tide-induced vertical motion remains influential even under moderate tidal conditions and may influence SAR-derived ice speed measurements on a broad range of Antarctic Ice Shelves.

Overall, these examples demonstrate that tide-induced apparent motion produces a spatially coherent signal in SAR-derived ice speed fields over floating Antarctic Ice Shelves which should be corrected if measurements of real ice speed variability are required. The magnitude and spatial extent of this signal depend jointly on regional tidal forcing, local tidal response and flow

https://doi.org/10.5194/egusphere-2026-3795
Preprint. Discussion started: 29 July 2026

direction with respect to SAR viewing geometry, with the largest correction magnitude occurring over extensive freely floating ice shelves exposed to strong tidal variability. The DROT-based tide correction largely removes the influence of this signal while preserving the underlying large-scale spatial pattern of ice flow and retaining other components of temporally variable ice speeds, thereby improving the physical consistency of short-repeat SAR-derived ice velocity products.

3.3 Temporal Variability of Tide-corrected Ice Speed Measurements

We investigated the degree to which tide-related offsets influence the temporal variability of short-repeat ice speed observations in Antarctica by extracting tide-corrected and uncorrected ice speed measurements along profiles on four representative Antarctic Ice Shelves (Figure 5). The two-dimensional density distributions were constructed using ice speed measurements processed from all available Sentinel-1 repeat image pairs acquired between October 2014 and December 2025, and therefore capture the cumulative short-term variability present within both the raw and tide-corrected ice speed products. The results show that tide-induced apparent motion systematically broadens the observed range of short-term ice speed variability over floating ice shelves. The effect is particularly pronounced over Larsen C (Figure 5b) and Brunt Stancomb (Figure 5c) Ice Shelves, where the raw velocity observations show a large spread across downstream floating regions. Following application of the DROT-based tide correction, the ice speed distributions substantially reduce into a narrower range, indicating that a large fraction of the apparent variability in the original ice speed measurements was caused by tide-driven range displacement rather than true short-term ice-dynamic change. On Larsen C Ice Shelf the mean temporal variability along the profile decreases by approximately 50 % following application of the tide correction (Table 1), while the upper 95th percentile tide correction magnitude exceeds 130 m/yr. On Brunt Stancomb Ice Shelf our results show a similarly large tide correction magnitude together with substantial narrowing of the temporal velocity distribution post tide correction. These results indicate that large tidal amplitudes can cause large temporal variability in short-repeat SAR-derived ice speed measurements over freely floating ice shelves if not corrected.

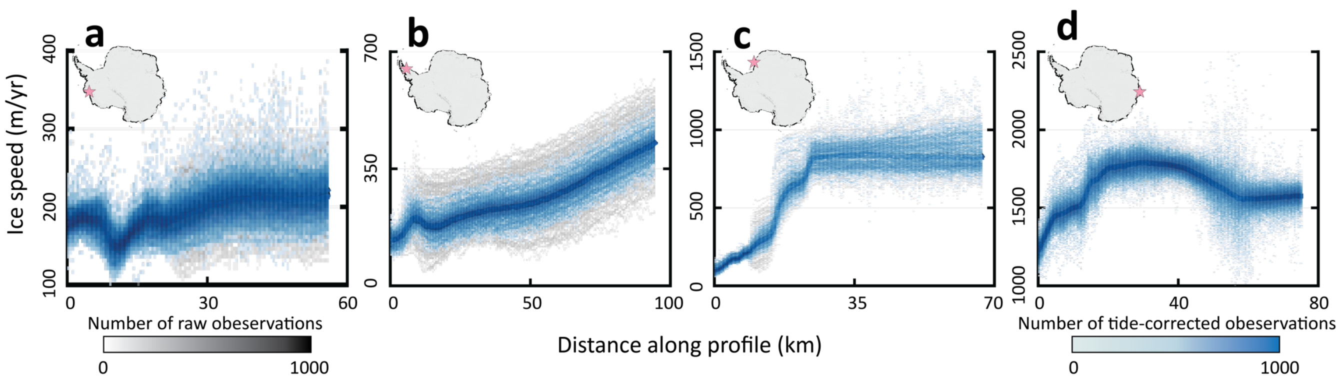

Figure 5. Temporal variability of ice-speed measurements extracted along profiles on Antarctic Ice Shelves before and after the application of a DROT-based tide correction. Two-dimensional density distributions of ice speed measurements were extracted along selected grounding-zone-crossing flowline profiles on four representative Antarctic Ice Shelves including (a) Pine Island; (b) Larsen C; (c)

https://doi.org/10.5194/egusphere-2026-3795
Preprint. Discussion started: 29 July 2026

Brunt Stancomb; and (d) Shackleton. Grey points represent the distribution of raw, uncorrected ice-speed observations, whereas blue points represent the corresponding tide-corrected ice speed measurements. The distributions were constructed using all available Sentinel-1 pairs throughout the satellite's observation period. Darker colours indicate a higher density of observations. Solid lines denote the median profile of each dataset. The profiles correspond to the transect locations shown in Figure 4, and the insets show the location of each profile in Antarctica.

In contrast, Pine Island (Figure 5a) and Shackleton (Figure 5d) Ice Shelves exhibit comparatively weaker modification of the temporally variable ice velocity distributions post tide correction. On Pine Island Ice Shelf, both the raw and tide-corrected ice speed observations already display relatively compact distributions which is consistent with the comparatively low tidal forcing present in the Amundsen Sea. Although localised corrections remain detectable, the overall temporal structure of the profile changes only modestly following application of the tide correction. Shackleton Ice Shelf exhibits intermediate behaviour, with moderate but systematic narrowing of the corrected ice velocity distribution despite more limited ocean tide forcing in the region compared with Larsen C or Brunt Stancomb Ice Shelves. Together, these examples demonstrate that the influence of tide-induced motion on SAR-derived ice speed depends strongly on the local tidal environment and the magnitude of ice shelf tidal response.

Overall, the temporal ice speed density distributions demonstrate that ocean tides represent a systematic source of short-term variability within SAR-derived Antarctic ice speed, which can be corrected if this signal is not required. By reducing the range of ice speed distributions, the DROT-based tide correction removes a potentially unwanted component of ice speed variability, which will facilitate the interpretation of real short-term ice speed variability measured using the offset-tracking technique while preserving the large-scale spatial structure of ice flow.

Table 1. Summary statistics of DROT-based tide correction magnitude and temporal variability reduction across representative Antarctic Ice Shelves.

Ice Shelf	Number of SLC pairs	Median correction (m/yr)	P95 correction (m/yr)	Variability reduction (%)
Pine Island	627	2.6	32.5	2.7
Larsen C	538	34.4	136.8	49.8
Brunt Stancomb	680	14.2	69.0	3.3
Shackleton	648	3.6	41.1	2.7

4.1 Validation using in situ GNSS Observations

We performed a comparison of Sentinel-1 satellite derived ice speed measurements and independent in situ GNSS observations collected on Brunt Stancomb Ice Shelf, to validate the performance of the DROT-based tide correction method (Figure 6). The GNSS dataset provides continuous measurements of ice displacement at a point location and therefore offers an independent

https://doi.org/10.5194/egusphere-2026-3795
Preprint. Discussion started: 29 July 2026

observational reference dataset for assessing the performance of the tide correction applied to satellite-based SAR-derived ice velocity products. As the DROT-based framework relies on externally derived sea-surface height variability, the accuracy of the tidal forcing fields was additionally evaluated by comparing the GNSS-derived vertical displacement with modelled tidal variability derived from the CATS2008 ocean tide model together with the ERA5-based inverse barometer correction (Figure S2). The comparison demonstrates strong agreement between GNSS-derived vertical motion and modelled sea-surface height variability. The CATS2008 tidal model alone reproduces the observed GNSS tidal signal with a correlation coefficient of approximately 0.98 and an RMSE of ~0.14 m. Incorporating ERA-5 based inverse barometer correction in the overall tide correction further improves the agreement, increasing the correlation coefficient to 0.99 and reducing the RMSE to ~0.12 m. These results indicate that the combined tidal and atmospheric-pressure correction provides a very reliable representation of short-term sea-surface height variability on Brunt Stancomb Ice Shelf and is therefore suitable for estimating tide-driven radar-range displacement within the DROT tide correction method.

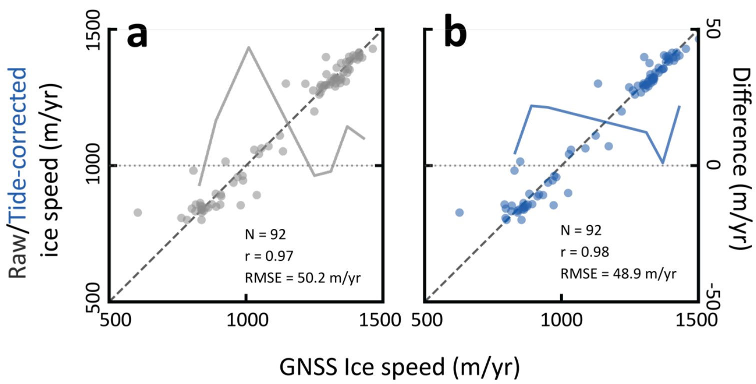

Figure 6. Validation of DROT-based tide-corrected ice speed using in situ GNSS observations. (a) Comparison between raw Sentinel-1 ice speed and in situ GNSS-derived ice speed measurements on Brunt Ice Shelf. (b) shows the same comparison as (a) but applied to DROT-based tide-corrected ice speed measurements. Each point represents one Sentinel-1 image pair, with in situ GNSS ice speed averaged over the corresponding acquisition interval. The dashed line indicates the 1:1 relationship, while the coloured lines referenced to the right-hand y-axis show the pairwise ice speed measurement difference between Sentinel-1 and GNSS observations.

Comparison between SAR-derived and GNSS-derived ice speed measurements further demonstrates the effectiveness of the tide correction method (Figure 6). Prior to correction, the Sentinel-1 ice-speed measurements already exhibit strong agreement with GNSS observations (r = 0.97), reflecting the overall robustness of offset-tracking velocity retrievals over floating ice shelves. However, the raw measurements display noticeable scatter around the 1:1 relationship, particularly during periods of large tidal variability, resulting in an RMSE of approximately 50.2 m/yr relative to the GNSS-derived speeds (Figure 6a). Following the application of the DROT-based tide correction, agreement between Sentinel-1 and GNSS observations improves further (Figure 6b). The corrected ice speeds remain highly correlated with the GNSS measurements (r = 0.98), while the scatter around the 1:1 relationship is reduced. The RMSE decreases from 50.2 to 48.9 m/yr, indicating that the tide correction

https://doi.org/10.5194/egusphere-2026-3795
Preprint. Discussion started: 29 July 2026

systematically removes the vertical displacement component of the ice speed variability which is associated with the difference in tidal state between SAR acquisitions. The relatively modest reduction in RMSE is expected because displacement associated with real ice flow remains the dominant large-scale component of ice motion and this is already well captured by the original offset-tracking measurements. Instead, the DROT-based tide correction primarily targets short-timescale variability associated with tide-induced apparent displacement, thereby reducing this variability which is superimposed on the background ice-flow field.

Our validation of the tide correction method through a comparison with in situ GNSS measurements demonstrates two important aspects of the DROT-based framework. First, the external tidal and atmospheric forcing fields reproduce observed short-term tidal variability with high accuracy. Second, incorporation of the DROT-derived tidal response coefficient reduces tide-induced variability in SAR-derived ice velocity measurements without degrading the underlying large-scale ice-flow signal. Together, these results provide independent observational support for the physical validity of the DROT-based tide correction approach.

4.2 Comparison with Elastic-model-based Approach

We compared our DROT-based tide correction with an elastic-beam model-based tide correction approach to provide insight into how an alternative but complementary tide correction method might be used to remove the influence of tidal variability on SAR-derived ice velocity products. Whereas the DROT framework estimates tidal response empirically from Sentinel-1 observations, the elastic-beam model-based approach (Wuite et al., 2026) derives tidal sensitivity from prescribed grounding geometry and elastic flexural theory. Our comparison shows the pairwise RMSE differences between a DROT-based and elastic-beam model-based tide-corrected ice velocity products across the four representative Antarctic Ice Shelves investigated in this study (Figure 7), with a corresponding statistical summary also provided (Table 2). Overall, both techniques perform very well with relatively small RMSE differences across all investigated regions, indicating that both approaches capture the dominant component of tide-induced velocity variability. Median RMSE differences generally range from ~1-3 m/yr, suggesting broad consistency between the two correction frameworks at large spatial scales.

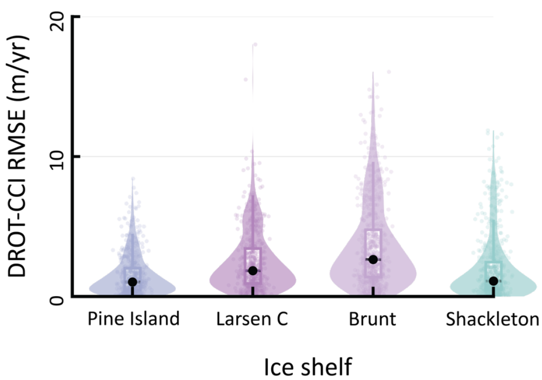

https://doi.org/10.5194/egusphere-2026-3795
Preprint. Discussion started: 29 July 2026

Figure 7. Comparison between DROT-based and elastic-beam-based tide corrections. RMSE differences between elastic-beam-based and DROT-based tide-corrected ice speed measurement pairs, on four Antarctic Ice Shelves (Pine Island, Larsen C, Brunt, and Shackleton). Each point represents an individual Sentinel-1 image pair, with RMSE calculated from all valid ice shelf pixels within the corresponding Sentinel-1 frame after applying grounding line and coastline mask. Violin widths indicate the probability density of RMSE values. Boxplots show the interquartile range and median, while black dots indicate the median RMSE of each ice shelf.

The smallest differences are observed on Pine Island Ice Shelf where the median RMSE difference remains close to ~1 m/yr and the distribution of pairwise RMSE values is relatively narrow (Figure 7; Table 2). This behaviour is consistent with the comparatively weak tidal forcing within the Amundsen Sea Sector and the smaller magnitude of the tide correction in this region, as previously shown (Figures 4 and 5). Under such conditions, tide-induced apparent motion represents only a relatively small component of the total observed displacement field, and both approaches therefore produce similar tide correction estimates and therefore a smaller difference. In contrast, substantially larger RMSE differences are observed on Larsen C and Brunt Stancomb Ice Shelves where the tidal amplitudes and correction magnitudes are considerably greater. Larsen C exhibits a broader RMSE distributions together with elevated upper-percentile values, while Brunt Stancomb Ice Shelf displays the largest overall disagreement between the two approaches (Figure 7). These regions exhibit strong spatial variability in tidal response associated with grounding zones and pinning points. Under such conditions, differences between idealized elastic flexure and observation-derived tidal response become increasingly important, leading to larger divergence between the two correction frameworks.

The observed differences likely arise from the fundamentally different assumptions underlying the two approaches. The elastic-beam model-based framework represents tidal flexure using prescribed grounding-line geometry, ice thickness, and idealized elastic beam behaviour, producing comparatively smooth spatial transitions in tidal response. In contrast, the DROT-based framework derives tidal sensitivity directly from observed radar-range displacement variability within the Sentinel-1 time series. Consequently, the DROT approach inherently captures localized spatial variability associated with grounding-zone migration, pinning points, and heterogeneous flexural behaviour that may not be fully represented using prescribed ice-shelf geometry alone.

Despite these methodological differences, the overall agreement between the two approaches remains strong across all investigated regions. Both methods substantially reduce tide-induced variability within SAR-derived velocity products while preserving the large-scale spatial structure of ice flow. The comparison therefore suggests that observation-driven approaches may provide particular advantages in regions where tidal response exhibits strong spatial heterogeneity that cannot be fully represented using idealized elastic flexure models alone, or in regions where the rate of ice shelf geometry changes outpace the availability of new observations, for example the case of grounding line retreat in the Antarctic Peninsula (Wallis et al., 2024). Because the DROT-based framework derives the tidal response directly from observations, it can also be updated as additional Sentinel-1 observations become available without requiring any modification to the underlying correction algorithm.

This flexibility makes the framework well suited to long-term operational ice velocity monitoring as the Sentinel-1 archive continues to expand.

Table 2. Statistical comparison between DROT-based and elastic-beam model-based tide correction approaches across representative Antarctic Ice Shelves.

Ice Shelf	Number of SLC pairs	RMSE difference (m/yr)
Pine Island	627	2.1
Larsen C	538	3.0
Brunt Stancomb	680	4.6
Shackleton	649	3.1

4.3 Implications for SAR-derived Ice Velocity Products

The results presented here demonstrate that tide-induced apparent motion represents a systematic source of short-term variability within SAR-derived ice velocity products over floating Antarctic Ice Shelves. In regions affected by strong tidal forcing, the apparent ice velocity fluctuations introduced by vertical tidal motion are significant and may reduce our ability to distinguish real short-term ice dynamic variability which is of particular interest for glaciological studies. Unless a tide correction is applied, some short-term ice speed variations measured using repeat-pass SAR observations may partly reflect differences in tidal state between acquisitions rather than real changes in ice dynamics. This effect is particularly relevant for studies investigating sub-seasonal variability in ice flow, grounding-zone migration, or short-term dynamic responses to calving and ocean forcing, where relatively small temporal changes in ice speed are often interpreted in terms of evolving ice shelf processes (Hogg et al., 2017; Boxall et al., 2022; Wallis et al., 2023b, a; Boxall et al., 2024).

The influence of tide-induced apparent motion is especially important for the interpretation of spatial velocity gradients over floating ice shelves. Grounding zones, pinning points, and shear margins are commonly characterized by strong spatial variability in ice motion and are therefore frequently analysed using velocity-derived strain rates and deformation fields (Rankl et al., 2017; Alley et al., 2018; Lhermitte et al., 2020; Wallis et al., 2024; Zhu et al., 2025). Because tidal response varies substantially across these regions, uncorrected tidal signals may locally modify the apparent spatial structure of SAR-derived ice velocity products and therefore influence the interpretation of localised deformation patterns. Correcting for tide-induced offsets, which is already common practice for altimetry based surface elevation change measurements on floating ice shelves (Shepherd et al., 2003; Hogg et al., 2021), consequently improves the physical interpretability of both temporal and spatial

https://doi.org/10.5194/egusphere-2026-3795
Preprint. Discussion started: 29 July 2026

variability in Antarctic ice velocity measurements and helps ensure that observed ice velocity gradients more accurately reflect underlying ice dynamics rather than transient tidal-state differences between SAR acquisitions.

The Antarctic-wide correction ranges identified in this study demonstrate that tide-induced apparent motion is not restricted to narrow grounding zone regions but extends across extensive downstream portions of freely floating Antarctic Ice Shelves. This has important implications for large-scale SAR-derived ice velocity products generated from dense Sentinel-1 time series, particularly those intended for continent-wide monitoring and temporal intercomparison. Because short-repeat SAR observations are increasingly used to construct monthly, seasonal and annually resolved Antarctic ice velocity datasets, uncorrected tidal variability may systematically influence the temporal consistency of derived products in regions affected by strong tidal forcing if uncorrected. Incorporating spatially distributed tide correction into operational SAR velocity-processing workflows therefore represents an important step toward improving the long-term consistency, inter-comparability and quality of Antarctic ice velocity products derived from modern short-repeat SAR observing systems.

Beyond the interpretation of ice velocity products themselves, improved tide correction also benefits a range of downstream applications that rely on high-quality ice velocity measurements. Surface velocity fields derived from dense Sentinel-1 observations are increasingly used to estimate basal melt rates through mass-conservation approaches, where errors in ice velocity propagate directly into inferred melt-rate distributions (Adusumilli et al., 2020; Davison et al., 2023). Reducing tide-induced biases therefore helps improve the physical consistency of basal melt estimates, particularly over floating ice shelves where tidal effects are strongest. Similarly, ice velocity products are widely used for model initialisation, data assimilation and stress-balance inversions within ice-sheet models, where observational consistency is essential for accurately representing present-day ice dynamics and constraining future projections (Nowicki et al., 2016; Seroussi et al., 2019, 2020). Enhanced temporal consistency of SAR-derived ice velocity fields consequently provides a more reliable observational basis for both process studies and predictive modelling of Antarctic Ice Sheet evolution. Once the tidal response coefficient has been estimated, the correction can be applied routinely to newly generated Sentinel-1 velocity products with only minimal additional computational cost, making the approach suitable for operational systems.

4.4 Future Work

The DROT-based framework presented here provides an observation-driven approach for estimating spatially variable tidal response directly from SAR time series. Future work should investigate how the tidal response itself evolves through time in response to changing ice shelf geometry, grounding line migration and calving-related reorganization of floating ice shelves. As the DROT-based framework derives tidal sensitivity empirically from repeat observations, the resulting tidal response fields may contain additional information regarding the evolving mechanical state of Antarctic Ice Shelves beyond their immediate application as a tide correction. Future studies should also explore the relationship between a DROT-derived tidal

https://doi.org/10.5194/egusphere-2026-3795
Preprint. Discussion started: 29 July 2026

response and other geophysical properties of floating ice shelves, including ice thickness, flexural rigidity, grounding zone structure and pinning point stability. Temporal changes in the tidal response may potentially provide indirect indicators of evolving ice-ocean interaction or change in basal coupling, particularly within dynamically active grounding zones and pinning point systems. Integrating a DROT-derived tidal response with interferometric measurements, altimetry observations and ice-ocean model outputs may provide additional opportunities to investigate the mechanical behaviour of Antarctic Ice Shelves. Such a multi-sensor approach could further improve our understanding of how changing ocean forcing influences grounding zone dynamics, flexural behaviour and basal coupling across floating ice shelves.

The increasing availability of temporally dense SAR observations from current and future satellite missions may further expand the applicability of observation-driven tide correction approaches. Continued Sentinel-1 acquisitions, together with forthcoming missions such as NASA-ISRO NISAR and Copernicus ROSE-L will provide increasingly extensive time series of short-repeat SAR observations over Antarctica using multiple radar frequencies (Iannini et al., 2024). Under such observing conditions, spatially and temporally variable tidal effects are likely to become increasingly important for interpreting short-term ice velocity variability from multi-frequency SAR approaches. Extending our observation-driven tide correction framework for multi-mission SAR datasets may therefore help improve the long-term consistency, physical interpretability and characterisation of uncertainties of Antarctic ice velocity products across different observing systems and acquisition geometries.

5 Conclusion

This study develops, applies and evaluates a DROT-based approach for correcting tide-induced apparent motion in Sentinel-1 offset-tracking ice velocity measurements over Antarctic Ice Shelves. We derive the tidal response coefficients directly from differential range offsets, providing an observation-driven method that accurately estimates the impact of local sea-surface height variability on radar-range displacement measurements without requiring prescribed ice thickness, grounding-line position, or elastic-beam parameterization. Application of the method across Antarctic Ice Shelves shows that tide-induced velocity corrections are spatially widespread and can be significant in magnitude. The Antarctic-wide tide correction range has a mean magnitude of 106 m/yr with standard deviation 71 m/yr, with maximum values exceeding 300 m/yr and more than 40% of ice-shelf pixels exceeding 100 m/yr. Large tide correction ranges occur mainly over freely floating ice shelves in regions of strong tidal forcing, particularly within the Weddell Sea and Antarctic Peninsula, whereas smaller values are found near grounding zones, pinning points and mechanically constrained regions where tidal motion is suppressed. The tide-induced signal in individual SAR image pairs can produce spatially coherent tide correction patterns in individual Sentinel-1 velocity fields. The magnitude of correction varies strongly between regions, with small tide corrections required over Pine Island Ice Shelf, larger tide corrections required over Larsen C and Brunt Stancomb. Time-series profile analyses shows that the DROT-based tide correction reduces temporal variability in SAR-derived ice speed associated with ocean tide signals, with the strongest reduction observed on the Larsen C Ice Shelf.

Independent validation using in situ GNSS observations on Brunt Stancomb Ice Shelf confirms that the tidal forcing represented by CATS2008 and ERA5-based inverse barometer correction agrees well with observed vertical motion. Comparison with GNSS-derived ice speed further indicates that DROT-based correction reduces variability in Sentinel-1 velocity estimates without degrading the underlying ice-flow signal. A comparison with an elastic-beam model-based tide correction shows broad consistency between the two approaches, while also highlighting differences in regions where tidal response is spatially complex such as the grounding zone. Overall, our results demonstrate that tide-induced apparent motion is an important source of short-term variability in short-repeat SAR-derived ice velocity products over floating Antarctic Ice Shelves. Applying a spatially distributed and temporally variable tide correction improves the physical consistency of short-repeat SAR-derived ice velocity products and facilitates more reliable interpretation of short-term Antarctic ice dynamic variability when a tide signal is not required.

Code and data availability

The code used to derive the DROT-based tidal response coefficient, together with the implementation for incorporating the tidal response coefficient into the SAR offset tracking workflow, and the Antarctic-wide DROT-derived tidal response coefficient dataset produced in this study are publicly available on Zenodo at https://doi.org/10.5281/zenodo.20815930.

Author contributions

YZ, AEH and BJW conceived the study, AEH, BJW, RAWS and YZ designed and implemented the ice velocity processing chain, YZ performed the analysis and wrote the paper. OJM provided GNSS data and contributed to the validation of the results. All authors discussed the results and contributed to the preparation of the paper.

Competing interests

The contact author has declared that none of the authors has any competing interests.

Acknowledgements

The authors gratefully acknowledge the European Space Agency (ESA) and the European Commission (EC) for the acquisition and availability of Copernicus Sentinel-1 data. This work used JASMIN, the UK's collaborative data analysis environment (https://www.jasmin.ac.uk).

https://doi.org/10.5194/egusphere-2026-3795
Preprint. Discussion started: 29 July 2026

Financial support

This work has been supported by the European Space Agency (ESA) 5D Antarctica project (grant no. 4000146702/24/I-KE) and the SUPSAR IV project (grant no. 4000148101/25/I-EB-bgh), and the Natural Environment Research Council (NERC) POLOMINTS (grant no. NE/Z000343/1).

References

Adusumilli, S., Fricker, H. A., Medley, B., Padman, L., and Siegfried, M. R.: Interannual variations in meltwater input to the Southern Ocean from Antarctic ice shelves, Nature geoscience, 13, 616–620, https://doi.org/10.1038/s41561-020-0616-z, 2020.

Alley, K. E., Scambos, T. A., Anderson, R. S., Rajaram, H., Pope, A., and Haran, T. M.: Continent-wide estimates of Antarctic strain rates from Landsat 8-derived velocity grids, Journal of Glaciology, 64, 321–332, https://doi.org/10.1017/jog.2018.23, 2018.

Bassis, J. N. and Jacobs, S.: Diverse calving patterns linked to glacier geometry, Nature Geoscience, 6, 833–836, https://doi.org/10.1038/ngeo1887, 2013.

Benn, D. I., Luckman, A., Åström, J. A., Crawford, A. J., Cornford, S. L., Bevan, S. L., Zwinger, T., Gladstone, R., Alley, K., Pettit, E., and others: Rapid fragmentation of thwaites eastern ice shelf, The Cryosphere, 16, 2545–2564, https://doi.org/10.5194/tc-16-2545-2022, 2022.

Boxall, K., Christie, F. D., Willis, I. C., Wuite, J., and Nagler, T.: Seasonal land-ice-flow variability in the Antarctic Peninsula, The Cryosphere, 16, 3907–3932, https://doi.org/10.5194/tc-16-3907-2022, 2022.

Boxall, K., Christie, F. D., Willis, I. C., Wuite, J., Nagler, T., and Scheiblauer, S.: Drivers of seasonal land-ice-flow variability in the Antarctic Peninsula, Journal of Geophysical Research: Earth Surface, 129, e2023JF007378, https://doi.org/10.1029/2023JF007378, 2024.

Brunt, K. M., Fricker, H. A., and Padman, L.: Analysis of ice plains of the Filchner–Ronne Ice Shelf, Antarctica, using ICESat laser altimetry, Journal of Glaciology, 57, 965–975, https://doi.org/10.3189/002214311798043753, 2011.

Davison, B. J., Hogg, A. E., Gourmelen, N., Jakob, L., Wuite, J., Nagler, T., Greene, C. A., Andreasen, J., and Engdahl, M. E.: Annual mass budget of Antarctic ice shelves from 1997 to 2021, Science Advances, 9, eadi0186, https://doi.org/10.1126/sciadv.adi0186, 2023.

Davison, B. J., Hogg, A. E., Slater, T., Rigby, R., and Hansen, N.: Antarctic Ice Sheet grounding line discharge from 1996–2024, Earth System Science Data, 17, 3259–3281, https://doi.org/10.5194/essd-17-3259-2025, 2025.

Dawson, G. J. and Bamber, J. L.: Measuring the location and width of the Antarctic grounding zone using CryoSat-2, The Cryosphere, 14, 2071–2086, https://doi.org/10.5194/tc-14-2071-2020, 2020.

De Zan, F. and Guarnieri, A. M.: TOPSAR: Terrain observation by progressive scans, IEEE Transactions on Geoscience and Remote Sensing, 44, 2352–2360, https://doi.org/10.1109/TGRS.2006.873853, 2006.

https://doi.org/10.5194/egusphere-2026-3795
Preprint. Discussion started: 29 July 2026

Dirscherl, M., Dietz, A. J., Dech, S., and Kuenzer, C.: Remote sensing of ice motion in Antarctica–A review, Remote Sensing of Environment, 237, 111595, https://doi.org/10.1016/j.rse.2019.111595, 2020.

Fricker, H. A. and Padman, L.: Ice shelf grounding zone structure from ICESat laser altimetry, Geophysical Research Letters, 33, https://doi.org/10.1029/2006GL026907, 2006.

Friedl, P., Weiser, F., Fluhrer, A., and Braun, M. H.: Remote sensing of glacier and ice sheet grounding lines: A review, Earth-Science Reviews, 201, 102948, https://doi.org/10.1016/j.earscirev.2019.102948, 2020.

Fürst, J. J., Durand, G., Gillet-Chaulet, F., Tavard, L., Rankl, M., Braun, M., and Gagliardini, O.: The safety band of Antarctic ice shelves, Nature Climate Change, 6, 479–482, https://doi.org/10.1038/nclimate2912, 2016.

Gourmelen, N., Kim, S. W., Shepherd, A., Park, J. W., Sundal, A. V., Björnsson, H., and Pálsson, F.: Ice velocity determined using conventional and multiple-aperture InSAR, Earth and Planetary Science Letters, 307, 156–160, https://doi.org/10.1016/j.epsl.2011.04.026, 2011.

Han, H. and Lee, H.: Tide-corrected flow velocity and mass balance of Campbell Glacier Tongue, East Antarctica, derived from interferometric SAR, Remote Sensing of Environment, 160, 180–192, https://doi.org/10.1016/j.rse.2015.01.014, 2015.

Hersbach, H., Bell, B., Berrisford, P., Biavati, G., Horányi, A., Muñoz Sabater, J., Nicolas, J., Peubey, C., Radu, R., and Rozum, I.: ERA5 hourly data on single levels from 1940 to present, Copernicus climate change service (c3s) climate data store (cds), 10, 24381, https://doi.org/10.24381/cds.adbb2d47, 2023.

Hogg, A. E.: Locating Ice Sheet Grounding Lines Using Satellite Radar Interferometry and Altimetry, PhD Thesis, University of Leeds, 2015.

Hogg, A. E., Shepherd, A., Cornford, S. L., Briggs, K. H., Gourmelen, N., Graham, J. A., Joughin, I., Mouginot, J., Nagler, T., and Payne, A. J.: Increased ice flow in Western Palmer Land linked to ocean melting, Geophysical Research Letters, 44, 4159–4167, https://doi.org/10.1002/2016GL072110, 2017.

Hogg, A. E., Gilbert, L., Shepherd, A., Muir, A. S., and McMillan, M.: Extending the record of Antarctic ice shelf thickness change, from 1992 to 2017, Advances in Space Research, 68, 724–731, https://doi.org/10.1016/j.asr.2020.05.030, 2021.

Howard, S. L., Erofeeva, S. Y., and Padman, L.: Cats2008: Circum-antarctic tidal simulation version 2008, 2019.

Howat, I., Porter, C., Noh, M.-J., Husby, E., Khuvis, S., Danish, E., Tomko, K., Gardiner, J., Negrete, A., Yadav, B., Klassen, J., Kelleher, C., Cloutier, M., Bakker, J., Enos, J., Arnold, G., Bauer, G., and Morin, P.: The Reference Elevation Model of Antarctica - Mosaics, Version 2, , https://doi.org/10.7910/DVN/EBW8UC, 2022.

Howat, I. M., Porter, C., Smith, B. E., Noh, M.-J., and Morin, P.: The reference elevation model of Antarctica, The Cryosphere, 13, 665–674, https://doi.org/10.5194/tc-13-665-2019, 2019.

Iannini, L., Davidson, M., Osborne, S., Gebert, N., Di Cosimo, G., Mezzasoma, S., Petrolati, D., Kazimierczak, D., Arranz, C. D. L. F., Miccoli, A., and others: ROSE-L-the copernicus expansion L-band SAR mission, in: EUSAR 2024; 15th European Conference on Synthetic Aperture Radar, 5–8, 2024.

Joughin, I., Tulaczyk, S., Bamber, J. L., Blankenship, D., Holt, J. W., Scambos, T., and Vaughan, D. G.: Basal conditions for Pine Island and Thwaites Glaciers, West Antarctica, determined using satellite and airborne data, Journal of Glaciology, 55, 245–257, https://doi.org/10.3189/002214309788608705, 2009.

https://doi.org/10.5194/egusphere-2026-3795
Preprint. Discussion started: 29 July 2026

Joughin, I., Shean, D. E., Smith, B. E., and Dutrieux, P.: Grounding line variability and subglacial lake drainage on Pine Island Glacier, Antarctica, Geophysical Research Letters, 43, 9093–9102, https://doi.org/10.1002/2016GL070259, 2016.

Joughin, I. A. N., Smith, B. E., and Howat, I. M.: A complete map of Greenland ice velocity derived from satellite data collected over 20 years, Journal of Glaciology, 64, 1–11, https://doi.org/10.1017/jog.2017.73, 2018.

Lemos, A., Shepherd, A., McMillan, M., Hogg, A. E., Hatton, E., and Joughin, I.: Ice velocity of jakobshavn isbræ, petermann glacier, nioghalvfjerdsfjorden, and zachariæ isstrøm, 2015–2017, from sentinel 1-a/b SAR imagery, The Cryosphere, 12, 2087–2097, https://doi.org/10.5194/tc-12-2087-2018, 2018.

Lhermitte, S., Sun, S., Shuman, C., Wouters, B., Pattyn, F., Wuite, J., Berthier, E., and Nagler, T.: Damage accelerates ice shelf instability and mass loss in Amundsen Sea Embayment, Proceedings of the National Academy of Sciences, 117, 24735–24741, https://doi.org/10.1073/pnas.1912890117, 2020.

Marsh, O., Rack, W., Floricioiu, D., Golledge, N. R., and Lawson, W.: Tidally induced velocity variations of the Beardmore Glacier, Antarctica, and their representation in satellite measurements of ice velocity, The Cryosphere, 7, 1375–1384, https://doi.org/10.5194/tc-7-1375-2013, 2013.

Marsh, O. J., Rack, W., Golledge, N. R., Lawson, W., and Floricioiu, D.: Grounding-zone ice thickness from InSAR: inverse modelling of tidal elastic bending, Journal of Glaciology, 60, 526–536, https://doi.org/10.3189/2014JoG13J033, 2014.

McMillan, M., Shepherd, A., Gourmelen, N., Dehecq, A., Leeson, A., Ridout, A., Flament, T., Hogg, A., Gilbert, L., Benham, T., and others: Rapid dynamic activation of a marine-based Arctic ice cap, Geophysical Research Letters, 41, 8902–8909, https://doi.org/10.1002/2014GL062255, 2014.

Miles, B. W. and Bingham, R. G.: Progressive unanchoring of Antarctic ice shelves since 1973, Nature, 626, 785–791, https://doi.org/10.1038/s41586-024-07049-0, 2024.

Nagler, T., Rott, H., Hetzenecker, M., Wuite, J., and Potin, P.: The Sentinel-1 mission: New opportunities for ice sheet observations, Remote Sensing, 7, 9371–9389, https://doi.org/10.3390/rs70709371, 2015.

Nowicki, S. M., Payne, A., Larour, E., Seroussi, H., Goelzer, H., Lipscomb, W., Gregory, J., Abe-Ouchi, A., and Shepherd, A.: Ice sheet model intercomparison project (ISMIP6) contribution to CMIP6, Geoscientific model development, 9, 4521–4545, https://doi.org/10.5194/gmd-9-4521-2016, 2016.

Otosaka, I. N., Horwath, M., Mottram, R., and Nowicki, S.: Mass balances of the Antarctic and Greenland ice sheets monitored from space, Surveys in Geophysics, 44, 1615–1652, https://doi.org/10.1007/s10712-023-09795-8, 2023.

Padman, L., Fricker, H. A., Coleman, R., Howard, S., and Erofeeva, L.: A new tide model for the Antarctic ice shelves and seas, Annals of Glaciology, 34, 247–254, https://doi.org/10.3189/172756402781817752, 2002.

Padman, L., Erofeeva, S., and Joughin, I. A. N.: Tides of the Ross sea and Ross ice shelf cavity, Antarctic Science, 15, 31–40, https://doi.org/10.1017/S0954102003001032, 2003.

Padman, L., Erofeeva, S. Y., and Fricker, H. A.: Improving Antarctic tide models by assimilation of ICESat laser altimetry over ice shelves, Geophysical Research Letters, 35, https://doi.org/10.1029/2008GL035592, 2008.

Padman, L., Siegfried, M. R., and Fricker, H. A.: Ocean tide influences on the Antarctic and Greenland ice sheets, Reviews of Geophysics, 56, 142–184, https://doi.org/10.1002/2016RG000546, 2018.

https://doi.org/10.5194/egusphere-2026-3795
Preprint. Discussion started: 29 July 2026

Palmer, S., Shepherd, A., Björnsson, H., and Pálsson, F.: Ice velocity measurements of Langjökull, Iceland, from interferometric synthetic aperture radar (InSAR), Journal of Glaciology, 55, 834–838, https://doi.org/10.3189/002214309790152573, 2009.

Rankl, M., Fürst, J. J., Humbert, A., and Braun, M. H.: Dynamic changes on the Wilkins Ice Shelf during the 2006–2009 retreat derived from satellite observations, The Cryosphere, 11, 1199–1211, https://doi.org/10.5194/tc-11-1199-2017, 2017.

Reese, R., Gudmundsson, G. H., Levermann, A., and Winkelmann, R.: The far reach of ice-shelf thinning in Antarctica, Nature Climate Change, 8, 53–57, https://doi.org/10.1038/s41558-017-0020-x, 2018.

Rignot, E.: Tidal motion, ice velocity and melt rate of Petermann Gletscher, Greenland, measured from radar interferometry, Journal of Glaciology, 42, 476–485, https://doi.org/10.3189/S0022143000003464, 1996.

Rignot, E., Mouginot, J., and Scheuchl, B.: Ice flow of the Antarctic ice sheet, Science, 333, 1427–1430, https://doi.org/10.1126/science.1208336, 2011.

Rignot, E., Mouginot, J., and Scheuchl, B.: MEaSUREs Antarctic Grounding Line from Differential Satellite Radar Interferometry, Version 2, , https://doi.org/10.5067/IKBWW4RYHF1Q, 2016.

Rignot, E., Mouginot, J., Scheuchl, B., Van Den Broeke, M., Van Wessem, M. J., and Morlighem, M.: Four decades of Antarctic Ice Sheet mass balance from 1979–2017, Proceedings of the National Academy of Sciences, 116, 1095–1103, https://doi.org/10.1073/pnas.1812883116, 2019.

Rott, H., Wuite, J., De Rydt, J., Gudmundsson, G. H., Floricioiu, D., and Rack, W.: Impact of marine processes on flow dynamics of northern Antarctic Peninsula outlet glaciers, Nature communications, 11, 2969, https://doi.org/10.1038/s41467-020-16658-y, 2020.

Selley, H. L., Hogg, A. E., Cornford, S., Dutrieux, P., Shepherd, A., Wuite, J., Floricioiu, D., Kusk, A., Nagler, T., Gilbert, L., and others: Widespread increase in dynamic imbalance in the Getz region of Antarctica from 1994 to 2018, Nature communications, 12, 1133, https://doi.org/10.1038/s41467-021-21321-1, 2021.

Selley, H. L., Hogg, A. E., Davison, B. J., Dutrieux, P., and Slater, T.: Speed-up, slowdown, and redirection of ice flow on neighbouring ice streams in the Pope, Smith, and Kohler region of West Antarctica, The Cryosphere, 19, 1725–1738, https://doi.org/10.5194/tc-19-1725-2025, 2025.

Seroussi, H., Nowicki, S., Simon, E., Abe-Ouchi, A., Albrecht, T., Brondex, J., Cornford, S., Dumas, C., Gillet-Chaulet, F., Goelzer, H., and others: initMIP-Antarctica: an ice sheet model initialization experiment of ISMIP6, The Cryosphere, 13, 1441–1471, https://doi.org/10.5194/tc-13-1441-2019, 2019.

Seroussi, H., Nowicki, S., Payne, A. J., Goelzer, H., Lipscomb, W. H., Abe-Ouchi, A., Agosta, C., Albrecht, T., Asay-Davis, X., Barthel, A., and others: ISMIP6 Antarctica: a multi-model ensemble of the Antarctic ice sheet evolution over the 21st century, The Cryosphere, 14, 3033–3070, https://doi.org/10.5194/tc-14-3033-2020, 2020.

Shepherd, A., Wingham, D., Payne, T., and Skvarca, P.: Larsen ice shelf has progressively thinned, Science, 302, 856–859, https://doi.org/10.1126/science.1089768, 2003.

Shepherd, A., Ivins, E., Rignot, E., Smith, B., van den Broeke, M., Velicogna, I., Whitehouse, P., Briggs, K., Joughin, I., Krinner, G., Nowicki, S., Payne, T., Scambos, T., Schlegel, N., A, G., Agosta, C., Ahlstrøm, A., Babonis, G., Barletta, V., Blazquez, A., Bonin, J., Csatho, B., Cullather, R., Felikson, D., Fettweis, X., Forsberg, R., Gallee, H., Gardner, A., Gilbert, L., Groh, A., Gunter, B., Hanna, E., Harig, C., Helm, V., Horvath, A., Horwath, M., Khan, S., Kjeldsen, K. K., Konrad, H., Langen, P., Lecavalier, B., Loomis, B., Luthcke, S., McMillan, M., Melini, D., Mernild, S., Mohajerani, Y., Moore, P., Mouginot, J., Moyano, G., Muir, A., Nagler, T., Nield, G., Nilsson, J., Noel, B., Otosaka, I., Pattle, M. E., Peltier, W. R., Pie, N., Rietbroek, R., Rott, H., Sandberg-Sørensen, L., Sasgen, I., Save, H., Scheuchl, B., Schrama, E., Schröder, L., Seo, K.-W., Simonsen, S., Slater, T., Spada, G., Sutterley, T., Talpe, M., Tarasov, L., van de Berg, W. J., van der Wal, W., van Wessem, M., Vishwakarma, B. D., Wiese, D., Wouters, B., and The IMBIE team: Mass balance of the Antarctic Ice Sheet from 1992 to 2017, Nature, 558, 219–222, https://doi.org/10.1038/s41586-018-0179-y, 2018.

Shepherd, A., Ivins, E., Rignot, E., Smith, B., van den Broeke, M., Velicogna, I., Whitehouse, P., Briggs, K., Joughin, I., Krinner, G., Nowicki, S., Payne, T., Scambos, T., Schlegel, N., A, G., Agosta, C., Ahlstrøm, A., Babonis, G., Barletta, V. R., Bjørk, A. A., Blazquez, A., Bonin, J., Colgan, W., Csatho, B., Cullather, R., Engdahl, M. E., Felikson, D., Fettweis, X., Forsberg, R., Hogg, A. E., Gallee, H., Gardner, A., Gilbert, L., Gourmelen, N., Groh, A., Gunter, B., Hanna, E., Harig, C., Helm, V., Horvath, A., Horwath, M., Khan, S., Kjeldsen, K. K., Konrad, H., Langen, P. L., Lecavalier, B., Loomis, B., Luthcke, S., McMillan, M., Melini, D., Mernild, S., Mohajerani, Y., Moore, P., Mottram, R., Mouginot, J., Moyano, G., Muir, A., Nagler, T., Nield, G., Nilsson, J., Noël, B., Otosaka, I., Pattle, M. E., Peltier, W. R., Pie, N., Rietbroek, R., Rott, H., Sandberg Sørensen, L., Sasgen, I., Save, H., Scheuchl, B., Schrama, E., Schröder, L., Seo, K.-W., Simonsen, S. B., Slater, T., Spada, G., Sutterley, T., Talpe, M., Tarasov, L., van de Berg, W. J., van der Wal, W., van Wessem, M., Vishwakarma, B. D., Wiese, D., Wilton, D., Wagner, T., Wouters, B., Wuite, J., and The IMBIE Team: Mass balance of the Greenland Ice Sheet from 1992 to 2018, Nature, 579, 233–239, https://doi.org/10.1038/s41586-019-1855-2, 2020.

Solgaard, A., Kusk, A., Merryman Boncori, J. P., Dall, J., Mankoff, K. D., Ahlstrøm, A. P., Andersen, S. B., Citterio, M., Karlsson, N. B., and Kjeldsen, K. K.: Greenland ice velocity maps from the PROMICE project, Earth System Science Data, 13, 3491–3512, https://doi.org/10.5194/essd-13-3491-2021, 2021.

Strozzi, T., Luckman, A., Murray, T., Wegmuller, U., and Werner, C. L.: Glacier motion estimation using SAR offset-tracking procedures, IEEE Transactions on Geoscience and Remote Sensing, 40, 2384–2391, https://doi.org/10.1109/TGRS.2002.805079, 2003.

Vaughan, D. G.: Tidal flexure at ice shelf margins, Journal of Geophysical Research: Solid Earth, 100, 6213–6224, https://doi.org/10.1029/94JB02467, 1995.

van de Wal, R. S., Boot, W., Van den Broeke, M. R., Smeets, C., Reijmer, C. H., Donker, J. J. A., and Oerlemans, J.: Large and rapid melt-induced velocity changes in the ablation zone of the Greenland Ice Sheet, science, 321, 111–113, https://doi.org/10.1126/science.1158540, 2008.

Wallis, B. J., Hogg, A. E., Meredith, M. P., Close, R., Hardy, D., McMillan, M., Wuite, J., Nagler, T., and Moffat, C.: Ocean warming drives rapid dynamic activation of marine-terminating glacier on the west Antarctic Peninsula, Nature Communications, 14, 7535, https://doi.org/10.1038/s41467-023-42970-4, 2023a.

Wallis, B. J., Hogg, A. E., van Wessem, J. M., Davison, B. J., and van den Broeke, M. R.: Widespread seasonal speed-up of west Antarctic Peninsula glaciers from 2014 to 2021, Nature Geoscience, 16, 231–237, https://doi.org/10.1038/s41561-023-01131-4, 2023b.

Wallis, B. J., Hogg, A. E., Zhu, Y., and Hooper, A.: Change in grounding line location on the Antarctic Peninsula measured using a tidal motion offset correlation method, The Cryosphere, 18, 4723–4742, https://doi.org/10.5194/tc-18-4723-2024, 2024.

Wuite, J., Nagler, T., Hetzenecker, M., and Rott, H.: Ten years of polar ice velocity mapping using Copernicus Sentinel-1, Remote Sensing of Environment, 332, 115092, https://doi.org/10.1016/j.rse.2025.115092, 2026.

https://doi.org/10.5194/egusphere-2026-3795
Preprint. Discussion started: 29 July 2026

Zhu, Y., Hogg, A. E., Hooper, A., and Wallis, B. J.: Short and Long-term Grounding Zone Dynamics of Amery Ice Shelf, East Antarctica, The Cryosphere, 19, 3971–3989, https://doi.org/10.5194/tc-19-3971-2025, 2025.